

Hybrid Stars in a Strong Magnetic Field

V. Dexheimer^{1,2}, R. Negreiros^{3,4}, and S. Schramm³

¹ UFSC, Florianopolis, Brazil

² Gettysburg College, Gettysburg, PA, USA

³ FIAS, Johann Wolfgang Goethe University, Frankfurt, DE

⁴ Instituto de Fisica, UFF, Av. Gal. Milton Tavares de Souza s/n. Gragoata, Niteroi, 24210-346, Brazil

Received: date / Revised version: date

Abstract. We study the effects of high magnetic fields on the particle population and equation of state of hybrid stars using an extended hadronic and quark SU(3) non-linear realization of the sigma model. In this model the degrees of freedom change naturally from hadrons to quarks as the density and/or temperature increases. The effects of high magnetic fields and anomalous magnetic moment are visible in the macroscopic properties of the star, such as mass, adiabatic index, moment of inertia, and cooling curves. Moreover, at the same time that the magnetic fields become high enough to modify those properties, they make the star anisotropic.

PACS. 97.60.Jd Neutron stars – 26.60.Dd Neutron star core – 26.60.Kp Equations of state of neutron-star matter – 25.75.Nq Quark deconfinement, quark-gluon plasma production, and phase transitions – 97.10.Ld Magnetic and electric fields

1 Introduction

Magnetars are compact stars that have surface magnetic fields up to $10^{14} - 10^{15}$ G [1,2]. Such fields can be estimated from observations of the star's period and period derivative. According to Virial theorem estimates, neutron stars could have a central magnetic field as large as 10^{18} or 10^{19} G. An accurate calculation of this limit is complicated, since all energies to be weighed against the magnetic energy (the one from matter and the gravitational one) also depend on the magnetic field (due to the nonlinear nature of General Relativity). For this reason the limit might be different for different equations of state (EOS's). Furthermore, due to the asymmetry introduced by the magnetic field in the z-direction, the pressure becomes different in the parallel and perpendicular directions. In reality, depending on the magnitude of the magnetic field, the parallel pressure becomes much smaller than the perpendicular one, and in extreme cases, can go locally to zero. In Ref. [3], as well as in our calculations, this limit was found to be around $10^{18} - 10^{19}$ G. Beyond this value strong instabilities can occur, which indicates that further investigation is necessary.

References [4,5] solve the Einstein and Maxwell equations self-consistently for non-rotating and rotating stars. They study axisymmetric and poloidal magnetic field configurations and find $B \sim 0.1$ to 4.2×10^{18} G as limits for the star central magnetic field. This range arises from the use of different hadronic EOS's, from a simple polytropic

to a hyperonic relativistic one. Although such EOS do not take into account magnetic field modifications, their formalism provides reliable results for star masses and radii because it takes into consideration different pressures in different directions of the star. It is important to notice that Ref. [6] states that the use of different current functions and symmetries, other than the axial one, together with effects of the magnetic field on the EOS may alter these limits. Other simulations including magnetic field effects can be found in [7,8,9,10].

It has also been shown by refs. [11,12] that using well accepted hadronic EOS's together with those based on first principles QCD calculations, one finds a phase transition to deconfined matter already at a few times saturation density inside compact stars. Such a phase transition can be a sharp first order transition or might exhibit a mixed phase, depending on the surface tension between the phases. In this work we study the effect of the latter.

There have also been works [13,14,15,16,17,18,19,20,21] showing that the inclusion of sophisticated quark coupling terms (like vector couplings, effective 6-quark interactions and quark-quark pairing) to the NJL and PNJL models, can lead to the appearance of a crossover chiral symmetry restoration/deconfinement phase transition at high density and small temperatures. In this case, the QCD phase diagram becomes more complicated due to the presence of a second critical point. Unfortunately, the values of the coupling constants which determine the precise nature of the phase transition in this regime are not predictable from first principles QCD calculations at this

Send offprint requests to:

point. Thus, the determination of the nature of the phase transition in this limit is still an active area of research.

One important question we will address is whether the effects of strong magnetic fields in the deconfinement phase transition are strong enough to be observed. Other studies along this line can be found in [22,23,24,25]. In order to do so in a realistic way, we adopt as our microscopic model a chiral approach that includes hadronic as well as quark degrees of freedom in a unified description [26,27,28]. Here, besides the analysis of the mass-radius diagram, we will extend our study to the adiabatic index and moment of inertia of the stars. Furthermore, we will, for the first time, investigate the thermal evolution of highly magnetized hybrid stars that include modifications in the EOS, which will help us to assess the effect of a high magnetic field on the cooling of the star. Finally, we will use two different approximations to take into account the pure magnetic field contribution to the energy density and pressure of the system. With this, we can model an EOS that is in principle anisotropic in an isotropic way and try to determine how reliable those approximations are.

2 The Model

Chiral sigma models are effective quantum relativistic models that describe hadrons interacting via meson exchange and, most importantly, are constructed from symmetry relations. They are constructed in a chirally invariant manner as the particle masses originate from interactions with the medium and, therefore, go to zero at high density and/or temperature. Adopting the nonlinear realization of the sigma model gives a significant improvement to the widely used linear sigma model [29,30] as it is in better agreement with nuclear physics results [31,32].

The Lagrangian density of the SU(3) non-linear sigma model in the mean field approximation constrained further by astrophysics data can be found in Ref. [33]. A recent extension of this model also includes quarks as dynamical degrees of freedom [26]. In this version, the degrees of freedom change due to the effective masses of the baryons and quarks. Their masses are generated by the scalar mesons (σ , isovector δ , strange ζ), except for a small explicit mass term M_0 and the term containing the field Φ . This field serves as an effective order parameter for the deconfinement transition and is modeled in such a way as to reproduce the behavior of the Polyakov loop at zero chemical potential, as determined by lattice QCD calculations [34]. The baryon and quark effective masses are given by

$$M_B^* = g_{B\sigma}\sigma + g_{B\delta}\tau_3\delta + g_{B\zeta}\zeta + M_{0B} + g_{B\Phi}\Phi^2, \quad (1)$$

$$M_q^* = g_{q\sigma}\sigma + g_{q\delta}\tau_3\delta + g_{q\zeta}\zeta + M_{0q} + g_{q\Phi}(1 - \Phi), \quad (2)$$

where the values for the coupling constants can be found in Ref. [26]. With the increase of density/temperature, the σ field (non-strange chiral condensate) decreases its value, causing the effective masses of the particles (in the absence of Φ) to decrease towards chiral symmetry

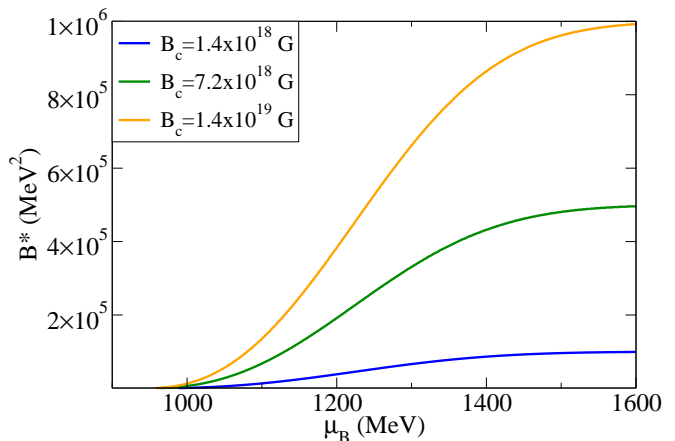


Fig. 1. (Color online) Effective magnetic field as a function of baryon chemical potential shown for different central magnetic fields.

restoration. The field Φ assumes non-zero values with the increase of temperature/density and, due to its presence in the baryons effective mass (Eq. (1)), suppresses the presence. On the other hand, the presence of the Φ field in the effective mass of the quarks, included with a negative sign (Eq. (2)), ensures that they will not be present at low temperatures/densities. The value for the g_Φ coupling constants is intrinsically related to the strength of the phase transition and only high values reproduce a first order phase transition at high densities and low temperatures.

Both phase transitions, chiral symmetry restoration (breaking) and deconfinement (confinement) happen at the same density/temperature. Such a fact comes from the correlation of these quantities in the effective masses of the particles. The potential for Φ reads

$$U = (a_0 T^4 + a_1 \mu_B^4 + a_2 T^2 \mu_B^2) \Phi^2 + a_3 T_0^4 \log(1 - 6\Phi^2 + 8\Phi^3 - 3\Phi^4). \quad (3)$$

This potential was modified from its original form in the PNJL model [35,36] by adding terms that depend on the baryon chemical potential. This allows us to reproduce the phase structure over the whole range of chemical potentials and temperatures, as suggested in lattice QCD studies [37,38], i.e. a cross over at small chemical potential and, at higher chemical potential, a first-order transition line that stops at a second-order critical end-point. Here, by using the modified μ_B dependent form for the Φ potential U , combined with a high value for the coupling of the Φ field for the hadrons and quarks, we obtain a first order phase transition at high densities, as it has been conjectured in other hybrid star calculations [39,40,41,42,43]. We stress again that this behavior is only a model assumption and, for instance in a Polyakov-extended quark-meson model [44] or in the quarkyonic picture [45] one might expect a smooth deconfinement crossover in this regime.

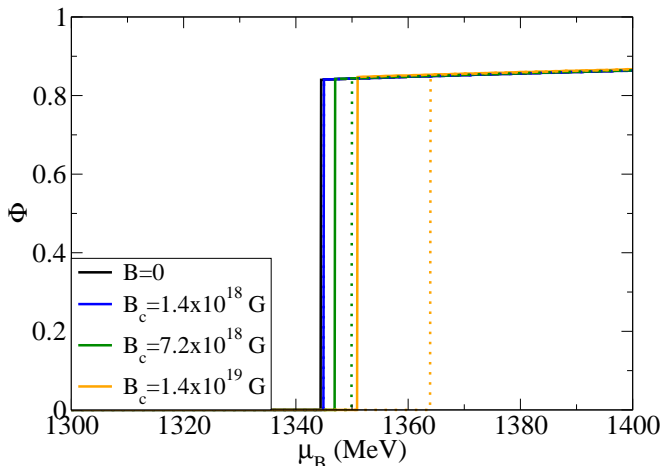


Fig. 2. (Color online) Deconfinement order parameter as a function of baryon chemical potential imposing local charge neutrality shown for different central magnetic fields. Dotted lines include AMM.

3 Inclusion of Magnetic Field

In order to have a more complete description of hybrid stars, we include magnetic fields that, while being in the z -direction, are not constant. The effective magnetic dipole field B^* increases with baryon chemical potential going from a surface value of $B_{surf} = 10^{15}$ G (when $\mu_B \simeq 938$ MeV) to a central value B_c at high baryon chemical potential

$$B^*(\mu_B) = B_{surf} + B_c \left[1 - e^{b \frac{(\mu_B - 938)^a}{938}} \right], \quad (4)$$

with $a = 2.5$, $b = -4.08 \times 10^{-4}$ and μ_B given in MeV. The use of the formula above generates no discontinuity in the effective magnetic field or in the increase of the effective magnetic field at the phase transition. Such an unphysical discontinuity would be present if we had chosen the effective magnetic field to be a function of baryon density, as is normally the case. The constants a , b and the form of B^* are chosen to reproduce (in the absence of quarks) the effective magnetic field curve as a function of density from Refs. [23, 46, 24]. As can be seen in Fig. 1, even with the use of extremely high central magnetic fields, the values for the effective magnetic fields only become extreme at very high baryon chemical potentials. In practice, only about 70% of B_c can be reached inside the star. Still, the highest central magnetic field considered in this work is above the limit established by hydrostatic stability from refs. [4, 5] and is only shown to illustrate the influence of an extreme high magnetic field in the EOS.

The magnetic field in the z -direction forces the eigenstates in the x and y directions of the charged particles to be quantized into Landau levels ν

$$E_{i\nu s}^* = \sqrt{k_{zi}^2 + \left(\sqrt{m_i^{*2} + 2\nu|q_i|B^*} - s_i\kappa_i B^* \right)^2}, \quad (5)$$

where k_i is the fermi momentum, q_i the charge and s_i the spin of each baryon or quark. The last term comes from the

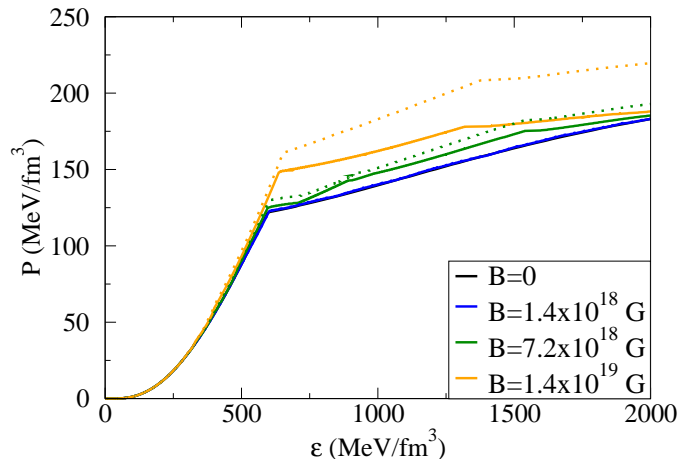


Fig. 3. (Color online) Equation of State (pressure of matter as a function of energy density of matter) assuming global charge neutrality for different central magnetic fields. Dotted lines include AMM.

anomalous magnetic moment (AMM) of the particle that splits the energy levels with respect to the alignment/anti-alignment of the spin with the magnetic field. The AMM also modifies the energy levels of the uncharged particles

$$E_{is}^* = \sqrt{k_i^2 + (m_i^{*2} - s_i\kappa_i B^*)^2}. \quad (6)$$

The constants κ_i determine the tensorial coupling strength of baryons with the electromagnetic field tensor and have values $\kappa_p = 1.79$, $\kappa_n = -1.91$, $\kappa_\Lambda = -0.61$, $\kappa_\Sigma^+ = 1.67$, $\kappa_\Sigma^0 = 1.61$, $\kappa_\Sigma^- = -0.38$, $\kappa_\Xi^0 = -1.25$, $\kappa_\Xi^- = 0.06$. The sign of κ_i determines the preferred orientation of the spin with the magnetic field. The sum over the Landau levels ν runs up to a maximum value, beyond which the momentum of the particles in the z -direction would be imaginary

$$\nu_{max} = \frac{E_{is}^{*2} + s_i\kappa_i B^* - m_i^{*2}}{2|q_i|B^*}. \quad (7)$$

We choose to include in our calculations the AMM effect for the hadrons only, since the coupling strength of the particles κ_i depends on the corresponding magnetic moment, that up to now is not fully understood for the quarks. Furthermore, it is stated in Ref. [47], that quarks in the constituent quark model have no anomalous magnetic moment. For calculations including AMM effects for the quarks see refs. [22, 48, 49, 50]. The AMM for the electrons is also not taken into account as its effect is negligibly small. Note that the AMM removes the spin degeneracy of the particles and their energy levels are further split in two levels each, which increases even more the particle chemical potentials.

As can be seen in Fig. 2, a phase transition which is of first order at zero temperature is delayed with the inclusion of high magnetic field. This effect is due to a stronger stiffening of the hadronic part of the EOS (as the magnetic field increases). The delay of the phase transition is further increased when the anomalous magnetic moment

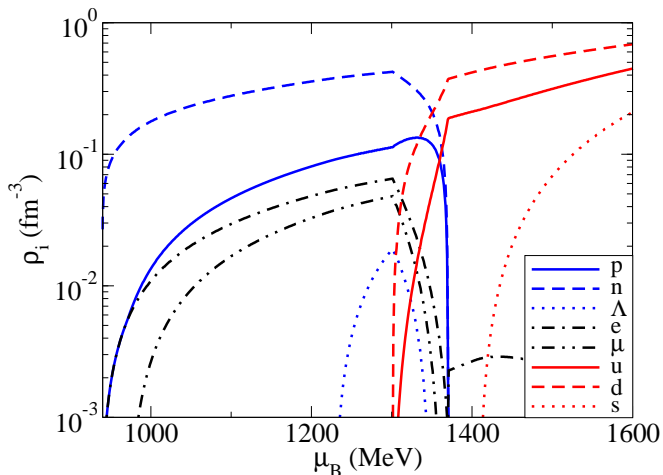


Fig. 4. (Color online) Particle densities as a function of baryon chemical potential assuming global charge neutrality for $B=0$. Quark densities are divided by 3.

is considered, as it only affects the hadronic phase, rendering its EOS stiffer (due an increase in the chemical potential of the baryons). If global charge neutrality is assumed, the location of the mixed phase does not change substantially, except for the highest magnetic field considered with AMM, when the entire mixed phase is pushed to slightly higher chemical potentials.

The same effect of confinement and/or chiral symmetry enhancement in the presence of high magnetic fields was already predicted by other works. In refs. [51,52,53] this was shown for high density and small or zero temperature, whereas in refs. [54,55,53,56] this was shown for small or zero density and high temperatures. Together, these features show the importance of the study of the influence of high magnetic fields and deconfinement/chiral symmetry restoration in compact stars as a part of a greater picture that forms the whole QCD phase diagram and contains heavy-ion experiments in the other extreme.

The EOS is shown in Fig. 3 for the case in which global charge neutrality is allowed and a mixed phase appears. We do not show the pure quark phase region, since in this model it is present only at very high densities that cannot be reached in the interior of stars. It is important to notice that at very low densities, the hadronic EOS of non-interacting matter gets softer in the presence of high magnetic field, in agreement with refs. [57,6] and other papers. In our case this effect is smaller because the magnetic field is only large at high densities. Note that only the energy density and pressure of matter are shown in this figure and no direct contribution from the magnetic field is included. In this way we can see the direct effects of the Landau quantization and the AMM in the model.

Fig. 4 shows the baryon density of fermions. In the mixed phase the hadrons disappear as the quarks smoothly appear. The hyperons, despite being included in the calculation, are suppressed by the appearance of the quark phase. Only a very small amount of Λ baryons appear right before the phase transition. The density of electrons and muons is significant in the hadronic phase but not

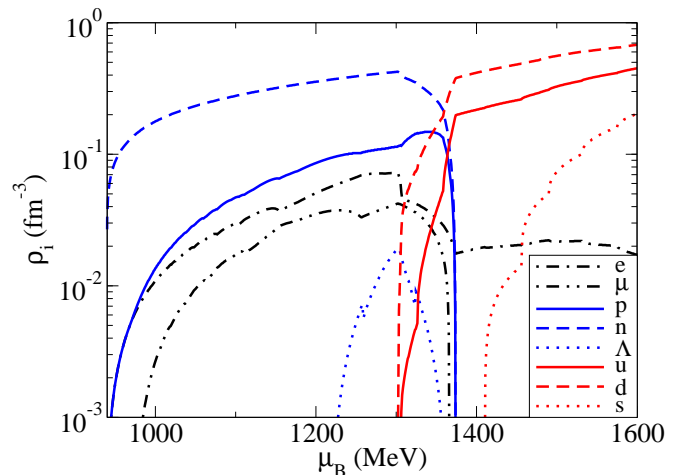


Fig. 5. (Color online) Particle densities as a function of baryon chemical potential assuming global charge neutrality for $B_c = 7.2 \times 10^{18}$ G, and including AMM. Quark densities are divided by 3.

in the quark phase. The reason for this behavior is that, because the down and strange quarks are also negatively charged, there is no necessity for the presence of electrons to maintain charge neutrality, and only a small amount of leptons remains to ensure beta equilibrium. The strange quarks appear after the other quarks, and do not make substantial changes in the system.

Fig. 5 shows the change in population when a central magnetic field of 7.2×10^{18} G with AMM is considered. The wiggles in the charge particle densities come from the Landau levels, more precisely when the Fermi energy of the particles crosses the discrete threshold of a Landau level. The charged particles are enhanced (as their chemical potentials increase with B), which is especially visible by the amount of electrons in the quark phase. The remaining hyperons are even more suppressed due to the increase in the proton density. All these effects are further enhanced when higher central magnetic fields are considered, like $B_c = 1.4 \times 10^{19}$ G.

4 Macroscopic Properties

A key point of this investigation is to determine whether the changes due to the presence of magnetic field in the EOS are strong enough to affect observable properties of the stars. To answer this question, we are going to analyze the adiabatic index, moment of inertia, mass-radius diagram and thermal evolution for different central magnetic fields.

4.1 Adiabatic Index

We begin with the adiabatic index (Fig. 6). The discontinuities in the $B = 0$ curve show the appearance of the Λ 's and the beginning of the mixed phase. The extra peaks in the finite magnetic field with AMM curves show the

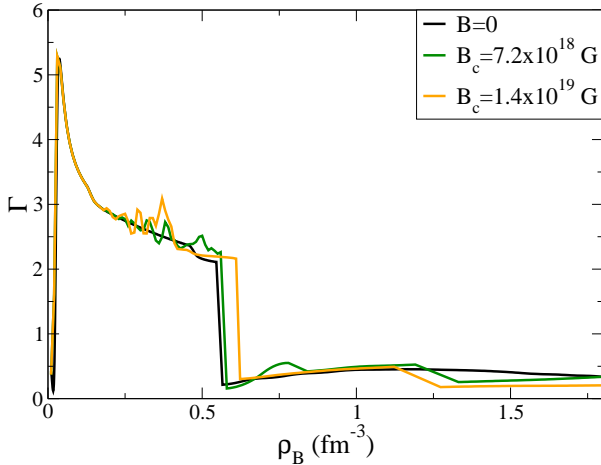


Fig. 6. (Color online) Adiabatic index as a function of baryon density for different central magnetic fields including AMM.

Landau level thresholds that also can be seen in the population plot. Note that the Landau level thresholds appear in the hadronic phase as well as in the mixed phase. As pointed out in Ref. [58], these rapid changes in the pressure can cause instabilities in the star that might cause star-quakes, glitches and giant flares.

4.2 Moment of Inertia

In Fig. 7 we show the moment of inertia as function of radius for several of the investigated stellar sequences, taking into account the AMM. We see that for the maximum central magnetic field considered (1.4×10^{19} G), there is an increase of about 10% from the unmagnetized case (for the maximum mass star). For $B_c = 7.2 \times 10^{18}$ G this increase is of about $\sim 2\%$. These results indicate that if the magnetic field of the object is changing, the moment of inertia will be modified, which might affect the spin evolution of the object, and might allow one to make a connection between AXP emission and glitches (see discussion in Ref. [58]). For lower central magnetic fields, the moments of inertia are almost the same as in the non-magnetized case.

4.3 Mass Radius Diagram

As a first approach to the problem, the possible hybrid star masses and radii are calculated by solving the Tolman-Oppenheimer-Volkoff equations for spherical isotropic static stars [59,60] using the EOS of matter. In Fig. 8, besides our EOS for the core, a separate EOS was used for the crust [61]. The maximum mass supported against gravity is higher for higher magnetic fields and even higher when the AMM is included. It is important to note that in this model pure quark matter only appears at very high densities, that correspond to the unstable branch of the mass-radius diagram. Thus, only hadronic and “mixed” matter appear in the star. Similar results for stars containing only hadronic and “mixed matter” were also found

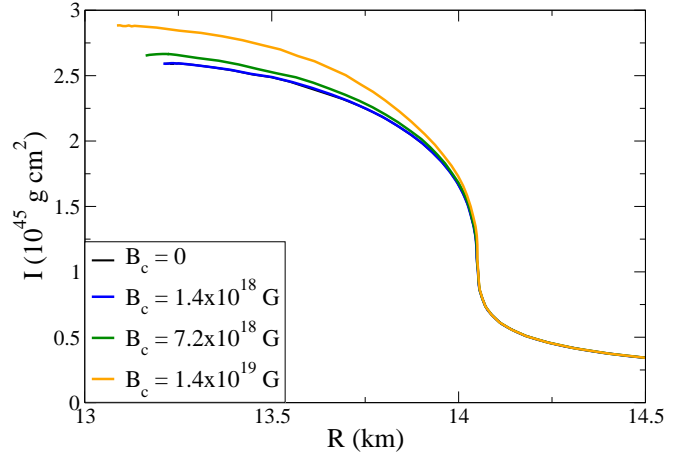


Fig. 7. (Color online) Moment of inertia as a function of radius for different central magnetic fields including AMM.

in a calculation using the Brueckner-Hartree-Fock model for the hadronic phase and the Dyson-Schwinger approach for the quarks [62].

So far, the magnetic field energy density and pressure contributions were not considered and only the influence of the magnetic field on the energy levels of the particles was taken into account. The problem in including the magnetic pressure is that it has different values in the directions parallel and perpendicular to the field, as can be seen in the electromagnetic energy-momentum tensor

$$T^{\mu\nu} = \frac{1}{4\pi} \begin{pmatrix} \frac{1}{2}B^{*2} & 0 & 0 & 0 \\ 0 & \frac{1}{2}B^{*2} & 0 & 0 \\ 0 & 0 & \frac{1}{2}B^{*2} & 0 \\ 0 & 0 & 0 & -\frac{1}{2}B^{*2} \end{pmatrix}, \quad (8)$$

where the first term is related to the energy density, the other three terms are related to the pressure in the x , y and z directions and the 4π comes from the choice of Gaussian natural units. This problem was pointed out in many papers such as refs. [63,64,49,50,65,3,66,25]. In these papers, there is also a term coming from the magnetic dipole interaction, which is linear in B and is therefore subleading at extremely high magnetic fields.

A consistent inclusion of the macroscopic magnetic pressure requires a 2D calculation. As mentioned before, such calculations exist [4,5]; however, most calculations performed using realistic EOS's for the macroscopic properties of magnetized stars assume isotropy and consider the pure magnetic pressure term to be either positive or negative in all directions. It was pointed out by refs. [23,67] that considering the magnetic pressure to be negative in all directions constrains the maximum values that can be used for the magnetic field to lower values. In our case, $B_c = 7.2 \times 10^{18}$ G would already cause an instability at very high densities. A third option, suggested by Ref. [68] uses, as a monopole approximation of the energy-momentum tensor, the average between the three pressures and adds $+B^2/24\pi$ for the magnetic pressure in all directions. We show the difference caused by either choosing the pure magnetic pressure to be positive in all

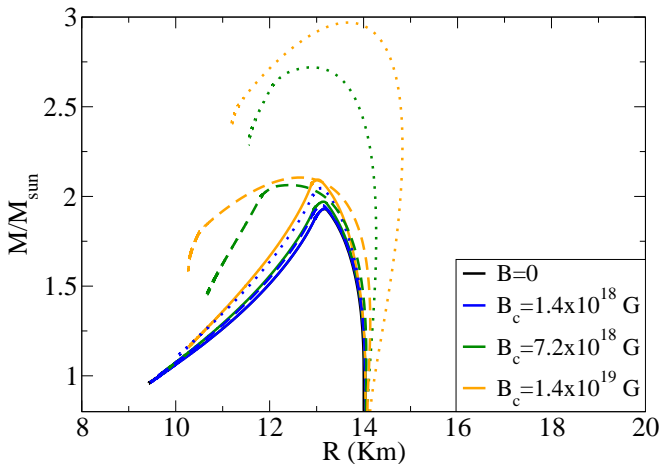


Fig. 8. (Color online) Mass-radius diagram shown for different central magnetic fields including AMM. The dashed and dotted lines have the extra magnetic pressure term of $B^{*2}/24\pi$ and $B^{*2}/8\pi$, respectively, added to the total pressure.

directions or using the average pressure in the mass-radius diagram. Evidently, the first case is unphysical (for extremily strong magnetic fields) since the magnetic pressure dominates over any other contribution. We speculate that the correct value would be close to the second option that uses the average of the pressures in different directions, but any more precise statement requires the use of axisymmetric equations, as was already pointed by Ref. [25]. Work along this line using our hybrid matter EOS is ongoing and will allow for a more exact estimate of the increase of the star mass based on the magnitude of the magnetic field of the magnetar.

4.4 Thermal Evolution

We now turn our attention to the thermal evolution of hybrid stars, whose microscopic composition is given by the model described in this paper. The cooling of compact stars is given by the thermal balance and thermal energy transport equation ($G = c = 1$) [69]

$$\frac{\partial(l e^{2\phi})}{\partial m} = -\frac{1}{\rho\sqrt{1-2m/r}} \left(\epsilon_\nu e^{2\phi} + c_\nu \frac{\partial(T e^\phi)}{\partial t} \right), \quad (9)$$

$$\frac{\partial(T e^\phi)}{\partial m} = -\frac{(l e^\phi)}{16\pi^2 r^4 \kappa \rho \sqrt{1-2m/r}}. \quad (10)$$

In Eqs. (9)–(10) the structure of the star is given by the variables r , $\rho(r)$, e^ϕ and $m(r)$, that represent the radial distance, the energy density, the metric function, and the stellar mass, respectively. The thermal variables are given by the temperature $T(r, t)$, luminosity $l(r, t)$, neutrino emissivity $\epsilon_\nu(r, T)$, thermal conductivity $\kappa(r, T)$, and specific heat $c_\nu(r, T)$. The boundary conditions of (9) and (10) are determined by the luminosity at the stellar center and at the surface. The luminosity vanishes at the stellar center since there is no heat flux there. The surface temperature (luminosity) is defined by the crust temperature

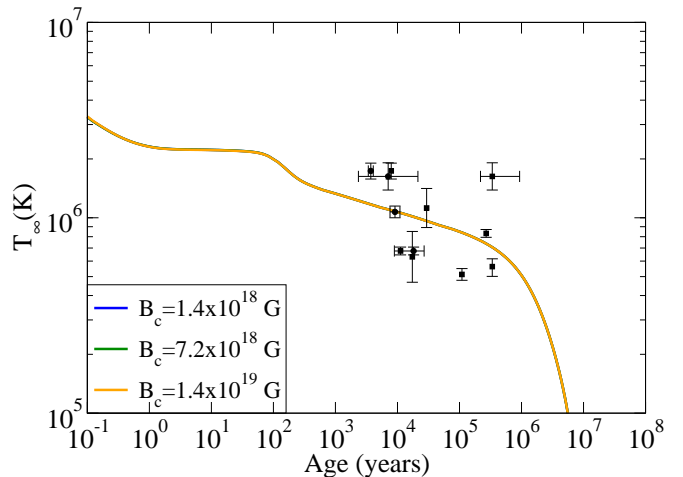


Fig. 9. (Color online) Cooling curves for a $1.1 M_\odot$ mass star in the presence of different central magnetic fields including AMM. T_∞ denotes the redshifted temperature observed at infinity. The observed data consists of circles denoting spin-down ages and squares denoting kinematic ages [76, 79]. The dashed and dotted lines include the extra magnetic pressure term of $B^{*2}/24\pi$ and $B^{*2}/8\pi$, respectively. All curves overlap.

and the properties of the stellar surface (surface gravity, magnetic field and etc.) [70, 71, 72, 73].

For the hadronic phase, we have considered the following neutrino emission processes: direct Urca, modified Urca and bremsstrahlung processes; whereas for the quark phase, the processes taken into account are the quark direct Urca, quark modified Urca, and quark bremsstrahlung processes. Details about the emissivities of such processes can be found in refs. [74, 75]. The specific heat of the hadrons is the usual specific heat of fermions, as described in Ref. [76]. As for the quarks, we use the expression for the specific heat calculated in Ref. [75]. The thermal conductivities for the hadronic and quark matter were calculated, respectively in refs. [77, 78], and in this work we follow the results presented in these references.

We have calculated the cooling for magnetized hybrid stars (with anomalous magnetic moment of the hadrons included) for three different masses: 1.1, 1.4 and $1.93 M_\odot$. For each hybrid star mass we considered three values for the central magnetic field (1.4×10^{18} , 7.2×10^{18} , 1.4×10^{19} G). In addition to that we have also considered the effect of including the pure magnetic field contribution in the EoS.

The cooling of $1.1 M_\odot$ stars is shown in Fig. 9. One can see that in this case the star exhibits a slow cooling, which agrees relatively well with the observed data. Furthermore, we can also conclude that in this case the magnetic field has no substantial effect on the thermal evolution of the object, and neither does the inclusion of the pure magnetic contribution in the EoS.

The situation is similar for stars with higher masses, as can be seen by the full lines in Figs. 10 and 11, which show the thermal evolution of stars with 1.4 and $1.93 M_\odot$, respectively. We see that in this case the modifications introduced by the magnetic field in the composition are not

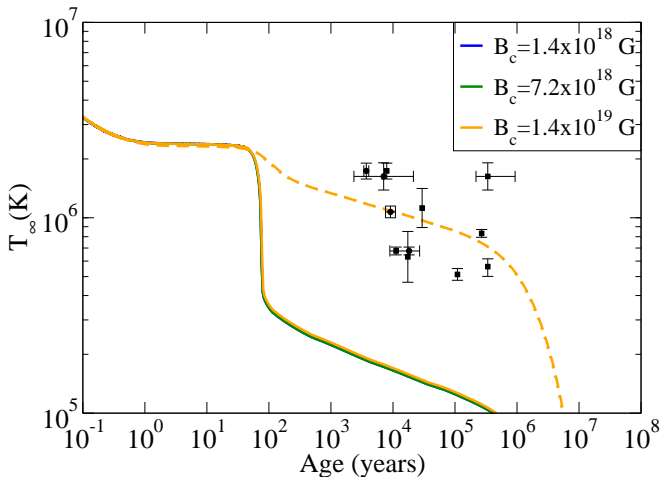


Fig. 10. (Color online) Cooling curves for a $1.4 M_{\odot}$ mass star. Otherwise same notation as Fig. 9. The dashed and dotted lines curves overlap.

enough to alter the cooling significantly (as was the case for lower mass stars). This picture changes, however, if one introduces the effect of the magnetic pressure. As shown by the dotted lines in Figs. 10 and 11, the extra $B^{*2}/8\pi$ leads to the slow cooling of a star that would otherwise exhibit fast cooling. This stems from the fact that adding an extra source of pressure stiffens the EoS. Hence, stars with higher masses possess smaller central densities and, therefore, smaller proton fractions. The small proton fraction will hinder the otherwise present direct Urca process, thus leading to a slow cooling. The results for the inclusion of the magnetic pressure of $B^{*2}/24\pi$ (dashed lines) are qualitatively the same. In this case, however, the stiffening of the EoS is more mild, and thus the effect is only appreciable for moderate masses, as seen in Fig. 10, where the thermal evolution is the same as for the magnetic pressure of $B^{*2}/8\pi$. For the $1.93 M_{\odot}$ star we see that the stiffening of the EoS is not enough to hinder the direct Urca process completely, and cooling of hybrid stars with magnetic pressure of $B^{*2}/24\pi$ is only slightly slower.

Note that in Figs. 9, 10 and 11 we have assumed an effective magnetic field that changes with density within the star but does not change in time. In a realistic scenario it is expected that the magnetic field decreases as a function of time as explained in Ref. [80,81,82]. In these references the authors also conclude that the inclusion of the magnetic field directly in the cooling simulation reproduces stars that remain warmer for a longer time, in better agreement with observation. On the other hand, such studies, do not include the effect of magnetic fields in the EOS, and therefore are complemented by our study.

4.5 Conclusions

To model magnetars, we use an effective model that includes hadronic and quarks degrees of freedom. As the density increases, the order parameters signal the deconfinement and chiral symmetry phase transitions, which

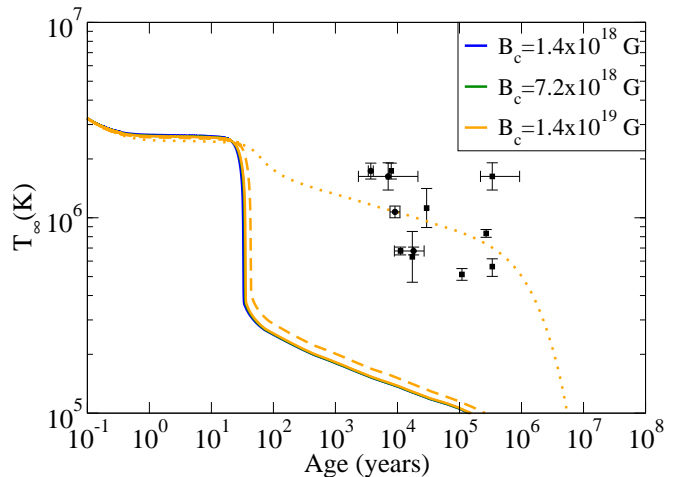


Fig. 11. (Color online) Cooling curves for a $1.93 M_{\odot}$ mass star. Otherwise same notation as Fig. 9.

tend to take place closer to the center of the star for higher magnetic fields. The stiffness of the equation of state (EOS), and the consequent star masses, depend on the chosen central magnetic field. It is clear that a higher B_c allows for more massive stars, but the quantitative analysis of how more massive the star might be requires the use of a 2D solution of Einstein's equations which takes into account the breaking of spherical symmetry by the magnetic field. This was shown by the dramatic change in the star masses when different assumptions were used for the inclusion of the pure magnetic field contribution to the EOS. As a consequence, only the lower magnetic field configuration with $B_c = 1.4 \times 10^{18}$ gives reliable results, as it has a pressure anisotropy $(p_z - p_{x,y})/(p_z + p_{x,y})$ of $\sim 20\%$. Having a 2D formalism will also allow to calculate the exact hydrodynamic limit for the magnetic field for our model. Efforts along these lines, using our EOS are currently taking place. In addition to the effect on the mass-radius relationship, we have shown that the presence of high magnetic fields can result in peaks in the adiabatic index and can modify the star's moment of inertia.

We introduce an expression for the effective magnetic field B^* that increases with baryon chemical potential, and therefore avoids a discontinuity in the phase transition region. This allows B^* to increase smoothly from a surface value up to a chosen central one (B_c). Furthermore, our investigation indicates that the composition changes introduced by the magnetic field are not high enough to alter significantly the thermal evolution of hybrid stars. We have found, however, that by including the magnetic pressure ($B^{*2}/8\pi$ or $B^{*2}/24\pi$), the consequent stiffening of the EoS allows for stars with higher masses ($1.4 - 1.93 M_{\odot}$) to exhibit slower cooling, which is in better agreement with the observed data. This is an important result, which indicates the importance of correctly introducing the macroscopic pressure into the structure of the star. We are cautious in interpreting these results, since the appropriate treatment of both the structure, and the thermal evolution of stars with such high magnetic fields requires a

full two-dimensional study [83]. We will save this investigation for a future work, as it seems clear to us that the effect of the magnetic pressure on the structure and thermal evolution are substantial. Although calculations which address this problem using model EOS's have already been performed, we believe that a well-motivated microscopic EOS that also includes the effects of the star's magnetic field is important for fully understanding the behavior of magnetars.

Subsequently, we would like to expand our study to finite temperature, in order to have a complete phase diagram (temperature as a function of baryon chemical potential) for high magnetic fields. A phase diagram for $B = 0$ was already constructed using the extended non-linear realization of the SU(3) sigma model in Ref. [26]. Such a complete analysis is important, since it connects the physics at high temperature and small densities such as those created in heavy ion collisions, with the physics inside neutron stars. A finite- B phase diagram was already constructed in Ref. [22] but we believe that we can give further insight into the matter with our model, since it also includes chiral symmetry restoration and allows for a smooth chiral and deconfinement crossover transition at small densities. It would also be interesting to study different parametrizations of the model which would give a smooth crossover in the low temperature regime and study the influence of the magnetic field in that case.

Acknowledgments

We are grateful to Constanca Providencia, Milva Orsaria, Fridolin Weber, Debora Menezes and Aurora Perez Martinez for the fruitful discussions on the subject of strong magnetic fields. R. N. acknowledges financial support from the LOEWE program HIC for FAIR. V. D. acknowledges financial support from CNPq-Brazil.

References

1. B. Paczynski, *Acta Astron.* **42**, 145 (1992)
2. A.I. Ibrahim, C. Markwardt, J. Swank, S. Ransom, M. Roberts et al., *AIP Conf.Proc.* **714**, 294 (2004)
3. E.J. Ferrer, V. de la Incera, J.P. Keith, I. Portillo, P.P. Springsteen, *Phys. Rev.* **C82**, 065802 (2010)
4. M. Bocquet, S. Bonazzola, E.ourgoulhon, J. Novak, *Astron.Astrophys.* **301**, 757 (1995)
5. C.Y. Cardall, M. Prakash, J.M. Lattimer, *Astrophys.J.* **554**, 322 (2001)
6. A.E. Broderick, M. Prakash, J.M. Lattimer, *Phys. Lett.* **B531**, 167 (2002)
7. V.C.A. Ferraro, *apsrev4-1* **119**, 407 (1954)
8. S. Lander, D. Jones, *Mon.Not.Roy.Astron.Soc.* **424**, 482 (2012)
9. L. Rezzolla, F.K. Lamb, S.L. Shapiro, *Astrophys.J.* **531**, L141 (2000)
10. K. Kiuchi, K. Kotake, *Mon.Not.Roy.Astron.Soc.* **385**, 1327 (2008)
11. A. Kurkela, P. Romatschke, A. Vuorinen, *Phys.Rev.* **D81**, 105021 (2010)
12. A. Kurkela, P. Romatschke, A. Vuorinen, B. Wu (2010), **1006.4062**
13. T. Hatsuda, M. Tachibana, N. Yamamoto, G. Baym, *Phys. Rev. Lett.* **97**, 122001 (2006)
14. G. Baym, T. Hatsuda, M. Tachibana, N. Yamamoto, *J.Phys.G* **G35**, 104021 (2008)
15. P. Powell, G. Baym, *The axial anomaly and three-flavor NJL model with confinement: constructing the QCD phase diagram*, in *APS Meeting Abstracts* (2012), p. 10001
16. N.M. Bratovic, T. Hatsuda, W. Weise (2012), **1204.3788**
17. O. Lourenco, M. Dutra, A. Delfino, M. Malheiro, *Phys.Rev.* **D84**, 125034 (2011)
18. O. Lourenco, M. Dutra, T. Frederico, A. Delfino, M. Malheiro, *Phys.Rev.* **D85**, 097504 (2012)
19. N. Yamamoto, M. Tachibana, T. Hatsuda, G. Baym, *Phys.Rev.* **D76**, 074001 (2007)
20. N. Yamamoto, *JHEP* **0812**, 060 (2008)
21. H. Abuki, G. Baym, T. Hatsuda, N. Yamamoto, *Phys.Rev.* **D81**, 125010 (2010)
22. S. Chakrabarty, *Phys. Rev.* **D54**, 1306 (1996)
23. D. Bandyopadhyay, S. Chakrabarty, S. Pal, *Phys. Rev. Lett.* **79**, 2176 (1997)
24. A. Rabhi, H. Pais, P.K. Panda, C. Providencia, *J. Phys.* **G36**, 115204 (2009)
25. L. Paulucci, E.J. Ferrer, V. de la Incera, J.E. Horvath, *Phys. Rev.* **D83**, 043009 (2011)
26. V.A. Dexheimer, S. Schramm, *Phys. Rev.* **C81**, 045201 (2010)
27. S. Schramm, R. Negreiros, J. Steinheimer, T. Schurhoff, V. Dexheimer, *Acta Phys.Polon.* **B43**, 749 (2012)
28. R. Negreiros, V. Dexheimer, S. Schramm, *Phys.Rev.* **C85**, 035805 (2012)
29. P. Papazoglou, S. Schramm, J. Schaffner-Bielich, H. Stoecker, W. Greiner, *Phys. Rev.* **C57**, 2576 (1998)
30. J.T. Lenaghan, D.H. Rischke, J. Schaffner-Bielich, *Phys. Rev.* **D62**, 085008 (2000)
31. P. Papazoglou et al., *Phys. Rev.* **C59**, 411 (1999)
32. L. Bonanno, A. Drago, *Phys. Rev.* **C79**, 045801 (2009)
33. V. Dexheimer, S. Schramm, *Astrophys. J.* **683**, 943 (2008)
34. K. Fukushima, *Phys. Lett.* **B591**, 277 (2004)
35. C. Ratti, M.A. Thaler, W. Weise, *Phys.Rev.* **D73**, 014019 (2006)
36. S. Roessner, C. Ratti, W. Weise, *Phys.Rev.* **D75**, 034007 (2007)
37. Z. Fodor, S. Katz, *JHEP* **0404**, 050 (2004)
38. Y. Aoki, G. Endrodi, Z. Fodor, S. Katz, K. Szabo, *Nature* **443**, 675 (2006), [hep-lat/0611014](#)
39. W. Lin, B.A. Li, J. Xu, C.M. Ko, D.H. Wen, *Phys.Rev.* **C83**, 045802 (2011)
40. C. Lenzi, A. Schneider, C. Providencia, R. Marinho, *Phys.Rev.* **C82**, 015809 (2010)
41. B. Agrawal, *Phys.Rev.* **D81**, 023009 (2010)
42. H. Chen, M. Baldo, G. Burgio, H.J. Schulze, *Phys.Rev.* **D84**, 105023 (2011)
43. T. Endo, *Phys.Rev.* **C83**, 068801 (2011)
44. T.K. Herbst, J.M. Pawlowski, B.J. Schaefer, *Phys.Lett.* **B696**, 58 (2011)
45. L. McLerran, R.D. Pisarski, *Nucl.Phys.* **A796**, 83 (2007)
46. G.J. Mao, A. Iwamoto, Z.X. Li, *Chin. J. Astron. Astrophys.* **3**, 359 (2003)
47. S. Weinberg, *Phys.Rev.Lett.* **65**, 1181 (1990)
48. I.S. Suh, G. Mathews, F. Weber, *Phys.Rev.D* (2001)

49. A. Perez Martinez, H. Perez Rojas, H.J. Mosquera Cuesta, M. Boligan, M.G. Orsaria, *Int. J. Mod. Phys.* **D14**, 1959 (2005)
50. R.G. Felipe, A.P. Martinez, H.P. Rojas, M. Orsaria, *Phys. Rev.* **C77**, 015807 (2008)
51. D. Menezes, M. Benghi Pinto, S. Avancini, A. Perez Martinez, C. Providencia, *Phys.Rev.* **C79**, 035807 (2009)
52. D. Menezes, M. Benghi Pinto, S. Avancini, C. Providencia, *Phys.Rev.* **C80**, 065805 (2009)
53. S.S. Avancini, D.P. Menezes, C. Providência, *Phys. Rev. C* **83**(6), 065805 (2011)
54. M. D'Elia, S. Mukherjee, F. Sanfilippo, *Phys.Rev.* **D82**, 051501 (2010)
55. A.J. Mizher, M. Chernodub, E.S. Fraga, *Phys.Rev.* **D82**, 105016 (2010)
56. R. Gatto, M. Ruggieri, *Phys.Rev.* **D83**, 034016 (2011)
57. A. Broderick, M. Prakash, J. Lattimer, *Astrophys.J.* (2000)
58. C.Y. Ryu, T. Maruyama, T. Kajino, G.J. Mathews, M.K. Cheoun, *Phys.Rev.* **C85**, 045803 (2012)
59. R.C. Tolman, *Phys.Rev.* **55**, 364 (1939)
60. J. Oppenheimer, G. Volkoff, *Phys.Rev.* **55**, 374 (1939)
61. G. Baym, C. Pethick, P. Sutherland, *Astrophys.J.* **170**, 299 (1971)
62. H. Chen, M. Baldo, G. Burgio, H.J. Schulze, *Phys.Rev.* **D84**, 105023 (2011)
63. M. Chaichian, S. Masood, C. Montonen, A. Perez Martinez, H. Perez Rojas, *Phys.Rev.Lett.* **84**, 5261 (2000)
64. A.P. Martinez, H. Rojas, H.J. Mosquera Cuesta, *Eur.Phys.J.* **C29**, 111 (2003)
65. A. Perez Martinez, H. Perez Rojas, H. Mosquera Cuesta, *Int. J. Mod. Phys.* **D17**, 2107 (2008)
66. M. Orsaria, I.F. Ranea-Sandoval, H. Vucetich, *Astrophys. J.* **734**, 41 (2011)
67. M. Sinha, B. Mukhopadhyay (2010), 1005.4995
68. I. Bednarek, A. Brzezina, R. Manka, M. Zastawny-Kubica, *Nucl.Phys.* **A716**, 245 (2003)
69. F. Weber, *Pulsars as astrophysical laboratories for nuclear and particle physics*, 1st edn. (Institute of Physics, Bristol, 1999)
70. E.H. Gudmundsson, C.J. Pethick, R.I. Epstein, *Astrophys. J. Lett.* **259**, L19 (1982)
71. E.H. Gudmundsson, C.J. Pethick, R.I. Epstein, *Astrophys. J.* **272**, 286 (1983)
72. D. Page, U. Geppert, F. Weber, *Nucl.Phys.* **A777**, 497 (2006)
73. D. Blaschke, T. Klahn, D. Voskresensky, *Astrophys.J.* **533**, 406 (2000)
74. D. Yakovlev, A. Kaminker, O.Y. Gnedin, P. Haensel, *Phys.Rept.* **354**, 1 (2001)
75. N. Iwamoto, *Annals of Physics* **141**, 1 (1982)
76. D. Page, J.M. Lattimer, M. Prakash, A.W. Steiner, *Astrophys.J.Suppl.* **155**, 623 (2004)
77. E. Flowers, N. Itoh, *Astrophys. J.* **250**, 750 (1981)
78. P. Haensel, *Nuclear Physics B Proceedings Supplements* **24**, 23 (1991)
79. D. Page, J.M. Lattimer, M. Prakash, A.W. Steiner, *Astrophys.J.* **707**, 1131 (2009)
80. D.N. Aguilera, J.A. Pons, J.A. Miralles, *Astrophys.J.* **673**, L167 (2008)
81. D.N. Aguilera, J.A. Pons, J.A. Miralles, *Astron.Astrophys.* **486**, 255 (2008)
82. Y. Xie, S.N. Zhang (2011), 1110.3869
83. R. Negreiros, S. Schramm, F. Weber, *Phys.Rev.* **D85**, 104019 (2012)